Specularity of longitudinal acoustic phonons at rough surfaces

Dhruv Gelda, Marc G. Ghossoub, Krishna Valavala, Jun Ma, and Manjunath C. Rajagopal
Department of Mechanical Science and Engineering, University of Illinois, Urbana, Illinois 61801, USA

Sanjiv Sinha*
Department of Mechanical Science and Engineering, University of Illinois, Urbana, Illinois 61801, USA
and Micro and Nanotechnology Laboratory, University of Illinois, Urbana, Illinois 61801, USA

(Received 29 November 2017; published 26 January 2018; corrected 14 September 2020)

The specularity of phonons at crystal surfaces is of direct importance to thermal transport in nanostructures and to dissipation in nanomechanical resonators. Wave scattering theory provides a framework for estimating wavelength-dependent specularity, but experimental validation remains elusive. Widely available thermal conductivity data presents poor validation since the involvement of the infinitude of phonon wavelengths in thermal transport presents an underconstrained test for specularity theory. Here, we report phonon specularity by measuring the lifetimes of individual coherent longitudinal acoustic phonon modes excited in ultrathin (36–205 nm) suspended silicon membranes at room temperature over the frequency range ∼20–118 GHz. Phonon surface scattering dominates intrinsic Akhiezer damping at frequencies $\gtrsim$60 GHz, enabling measurements of phonon boundary scattering time over wavelengths ∼72–140 nm. We obtain detailed statistics of the surface roughness at the top and bottom surfaces of membranes using HRTEM imaging. We find that the specularity of the excited modes are in good agreement with solutions of wave scattering only when the TEM statistics are corrected for projection errors. The often-cited Ziman formula for phonon specularity also appears in good agreement with the data, contradicting previous results. This work helps to advance the fundamental understanding of phonon scattering at the surfaces of nanostructures.

DOI: 10.1103/PhysRevB.97.045429

I. INTRODUCTION

Recent measurements of thermal transport in nanostructures have motivated a reexamination of the specularity of phonons' scattering at surfaces. Specularity is difficult to measure directly in heat conduction experiments. Instead, a standard empirical approach is to assume an effective specularity [1] across all phonon modes without considering any wavelength dependence. Within this approach, perfectly diffuse scattering (zero specularity) satisfactorily appears to explain the majority of thermal conductivity data [2] in structures with characteristic dimensions larger than ∼0.5 μm. Since dominant phonon wavelengths at room temperature approach a few nm and are comparable to the typical cleanroom processed surface roughness, diffuse scattering appears physically reasonable at room temperature. However, it is difficult to argue that phonons should scatter diffusely from similar surfaces even at low temperatures. The gap in understanding wavelength-dependent surface scattering is evident in the confusion over transport in more complicated nanostructures such as metal-assisted chemically etched nanowires, core-shell nanowires, or holey silicon [3–6]. The failure of the effective approach in these select cases has prompted a theoretical examination of the wavelength dependence in phonon surface scattering [7–9]. The availability of systematic data on specularity, however, remains a challenge.

Specularity of a surface to an incident wave depends on the relative magnitude of the wavelength to the roughness height and correlation length [10]. The exact dependence can vary substantially based on simplifying assumptions. Which theoretical results from wave scattering theory could be applied to phonon transport remains unclear. A recent innovative measurement [11] using superconducting tunnel junctions to identify individual phonon frequencies found zero specularity for phonons incident at nm scale roughness, even at $\lesssim$0.1 THz frequencies. Interestingly, the report found that the measured zero specularity was inconsistent with that predicted by a formula based on the Rayleigh-Rice theory [9,12] (also referred to as the Ziman formula in the phonon transport literature [13]). The formula applies in the limit of an infinite correlation length, and under the assumption of small roughness in relation to the incident wavelength. The specularity is then given by $e^{-16\pi^2\eta^2/\lambda^2}$ where η is the root mean square height of surface roughness and λ is the wavelength. In contrast, in another experiment [14] on coherently excited phonon modes in silicon membranes, the Ziman expression was used to fit data in the similar frequency range (20–500 GHz). The lack of detailed statistics of surface roughness in either measurement further makes data interpretation difficult. In this paper, we show that the roughness statistics from detailed surface characterization is necessary to interpret boundary scattering data. Distinct from these measurements, we find that phonons in the measured 20–118 GHz range reflect specularly for surfaces with typical $\lesssim$1 nm roughness. These sub-THz frequencies are important for nanomechanical

*sanjiv@illinois.edu

resonators and thermal transport at low and intermediate temperatures.

To verify phonon specularity against expectations from wave scattering theory, this work combines detailed surface characterization using high resolution transmission electron microscopy (HRTEM), with measurements of phonon lifetimes of longitudinal acoustic modes. Long-window HRTEM of roughness profiles enable us to obtain detailed roughness statistics across multiple membranes. A subtle error arises in projecting the two-dimensional roughness of the surface to a one-dimensional profile measured by the HRTEM. We find that correcting the error is critical toward matching wave theory predictions against the experimental data. In the optical measurements, individual phonon modes are coherently excited in the frequency range ∼20–118 GHz in ultrathin suspended Si membranes (∼36–205-nm thick) using an ultrafast laser pump. The suspended membrane acts as nanomechanical resonator in our experiments. The quality factor (Q) of the resonator is intrinsically limited by scattering with phonons [15–17]. However, extrinsic processes [18] such as surface scattering dominates attenuation in practice. In our experiments, we measure the attenuation of each mode using a time-delayed probe to find that intrinsic Akhiezer damping correctly predicts phonon lifetimes at the lower frequencies ($\nu \leqslant 24$ GHz), consistent with results for bulk silicon [19]. The reduction in phonon lifetimes at higher frequencies ($\geqslant$60 GHz), however, is dominated by roughness-dependent phonon surface scattering. We analyze the lifetime data using results from wave scattering theory at rough surfaces [9,10,20–22] and find that the estimated phonon specularities are in good agreement with the data over the measured frequency range.

II. EXPERIMENT

For our measurements, we fabricated free-standing single-crystal silicon membranes from the [100]-oriented silicon-on-insulator (SOI) wafers [23]. The device layer, buried oxide, and the Si substrate are 205-nm, 410-nm, and 700-μm thick, respectively. We first deposited a 300-nm-thick film of silicon nitride (SiN_x) on top of the device layer using a low pressure chemical vapor deposition (LPCVD) process at 800° C. To reduce the surface damage and contamination in subsequent fabrication process, we encapsulated the diced SOI samples with protective silicon dioxide and SiN_x layers using plasma-enhanced chemical vapor deposition (PECVD). We then defined a backside window using photolithography and etched the Si substrate using a combination of deep reactive ion etching (DRIE—Inductively coupled Bosch Process) and wet etching in tetramethylammonium hydroxide (TMAH: 80° C). The buried oxide layer is removed by placing the samples in a buffered oxide etch (BOE) solution. Silicon membranes are suspended by removing the protective layers covering the top surface of the SOI samples using Freon RIE. Further etching with the same Freon RIE process allowed us to control the thickness of the membrane to within ∼10 nm. The approach yielded membranes of ∼300 μm× ∼ 400 μm area with thicknesses in the range 36–205 nm.

We perform lifetime measurements using an ultrafast laser pump-probe setup which was described in detail previously [24–26]. Both the pump and probe beams are obtained from a synchronously mode-locked Ti:sapphire oscillator with a repetition rate of 74.8 MHz, pulse duration of 200 fs, and a wavelength of 785 nm. The pump beam is modulated using an electrooptic modulator at 10 MHz to facilitate lock-in detection of the reflected probe beam. The $1/e^2$ radius of the focused pump and probe spots on the sample surface is ∼5.5 μm. The pump pulses hitting the sample surface create an electron-hole (e-h) plasma, which after relaxation (∼1 ps) [27] creates stress in the illumination region of the membrane [28]. The generated stress is uniform along the thickness of the membrane due to the large penetration depth [29] (∼8 μm) of 785-nm wavelength in silicon and results in excitation of the first-order dilatation mode of the membrane. The frequency of oscillation is given by $\nu = V_L/2d_0$, where $V_L = 8430$ m/s is the longitudinal speed of sound in silicon [30] and d_0 is the thickness of the membrane. The excited acoustic mode modulates the membrane thickness ($\Delta d_0 < 1$ pm), which, in turn, changes the reflectivity of the membrane ($\Delta R/R \sim 10^{-5}$) [14,31] measured by the probe beam. Varying the delay between the arrival of the pump and the probe beams captures the time evolution of the amplitude of the excited acoustic mode.

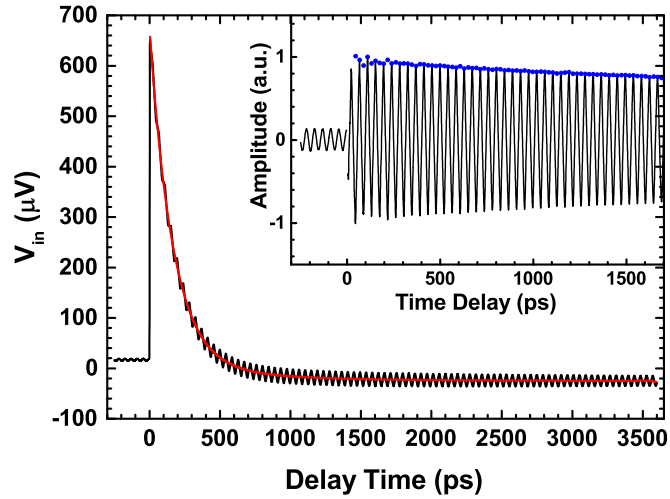

FIG. 1. In-phase voltage (black) obtained from pump-probe measurements for 182-nm-thick membrane. The slowly decaying electronic background (red) is fitted using a spline. (Inset) Acoustic signal extracted after removing the electronic background from the in-phase voltage.

Figure 1 shows the in-phase voltage obtained from the lock-in amplifier for a 182-nm-thick membrane which corresponds to 23.1 GHz longitudinal acoustic mode. The sharp rise in the signal at $t = 0$ ps is due to electronic excitation followed by a multi-exponential decay. The electronic response is removed to obtain the acoustic modes [32] shown in the inset of Fig. 1. We detect the peaks in the resulting acoustic signal and use linear regression to fit a line through the logarithm of the peak amplitudes. The amplitude damping time is obtained from the inverse of the slope of fitted line. The phonon lifetime (τ) is defined as the rate of energy decay and is half of the amplitude damping time (since acoustic energy scales as the square of the amplitude).

To facilitate a quantitative evaluation of boundary scattering in the measured thin films, we characterize the roughnesses of the top and bottom surfaces of the membranes in terms

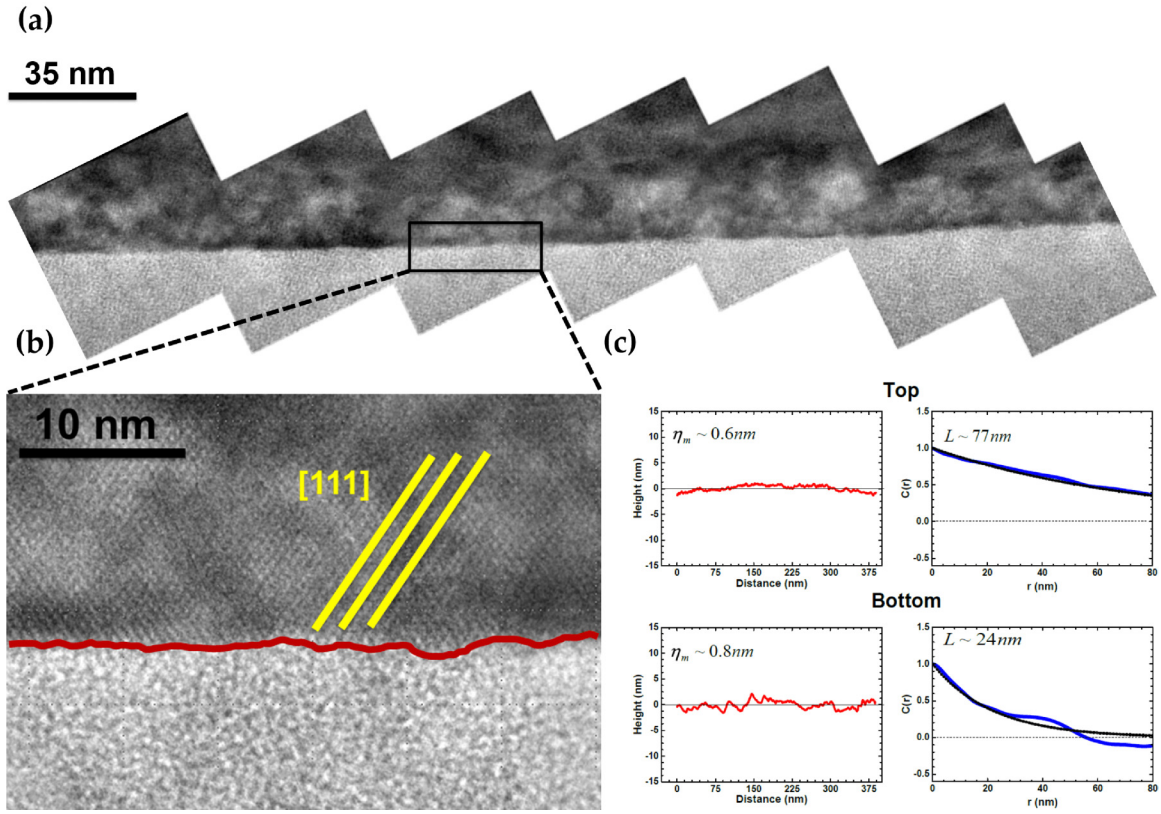

FIG. 2. (a) Example of a stitched surface roughness profile for the top surface of a silicon membrane obtained from TEM. (b) High resolution TEM micrograph along the (110) zone axis with crystalline Si membrane at the top, Pt/C composite at the bottom, and native SiO_2 in between. The red line traces the Si-SiO_2 interface at the surface of the membrane. (c) Surface roughness profile (left) and the corresponding autocorrelation function (right) for the top and bottom surfaces of a membrane with 187-nm thickness. The blue line represents the measured autocorrelation function and the black curve represents the exponential fit.

of the correlation length, L, and the root mean square (rms) roughness height, η. We use a JEOL 2010 LaB_6 transmission electron microscope (TEM) to obtain roughness profiles for five membrane samples with thicknesses of 36, 49, 132, 175, and 187 nm. The sample preparation for TEM imaging includes depositing 100 nm copper on the bottom surface of the membrane for reinforcement and 200 nm Pt/C composite on the top surface. We used electron-beam-induced deposition on the top side to prevent damage to the surface of the membrane [33]. We slice a thin (∼100-nm width) rectangular portion of the membrane and transfer it to the TEM grid inside a FIB. The cross section of the membrane is then imaged in 40–60 nm segments along the (110) zone axis to obtain a series of high resolution (400K X) images. The individual images are stitched together [Fig. 2(a)] using ImageJ [34] to obtain a surface profile over distances of ∼350–450 nm. The [111] direction serves as a reference to establish correspondences between adjacent pairs of images during the stitching process. The interface boundary [Fig. 2(b)] is traced by selecting discrete points corresponding to the last discernible Si lattice site along the [111] direction. The surface roughness profile [Fig. 2(c), left column] is then obtained by interpolating over the unequally spaced discrete points with a smoothing B-spline at a sampling interval $\geqslant$0.3 nm.

To determine the correlation length L from the surface roughness profile, we first evaluate the height-height autocorrelation function (ACF). Following prior work on understanding electron scattering at the Si-SiO_2 interface [35,36], we fit the decay of the ACF as an exponential distribution of the form $C(r) = \exp(-r/L)$ and extract the correlation length L as shown in the right column of Fig. 2(c). We find that the measured correlation length lies in the range $L \sim$ 6–77 nm between different membranes. Since the lengths are measured using a finite picture window, we expect a compression of the correlation length and rms roughness between the actual and measured values [36], especially when the correlation length is comparable to the window length. To avoid this issue, we use long window lengths of ∼375 nm beyond which we lost TEM focus. We find that the measured values for L are $\leqslant$20% of the window length, and therefore, the finite window does not introduce any significant compression in L. We note that our measurements obviously cannot resolve correlation lengths longer than the window length of 375 nm. We also obtain the rms roughness height of the membrane samples from the standard deviation of the surface roughness profile. The measured rms roughness, η_m range from 0.4 to 1.3 nm.

A subtle issue with obtaining surface roughness from HRTEM images is that the images are one-dimensional projections of the two-dimensional roughness, through the membrane cross-section [36]. Previous measurements [36,37] on Si-SiO_2 interfaces with similar surface treatment reported that rms roughness extracted from the projection, η_m are lower than the actual roughness, η. To account for any such reduction, we numerically obtained a correction factor for every

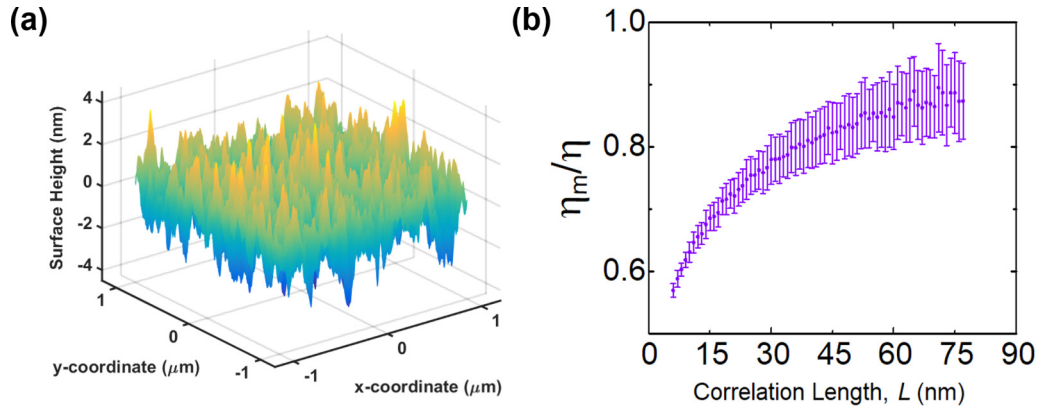

FIG. 3. (a) Two-dimensional random rough surface generated using exponential statistics for rms roughness $\eta = 1.0$ nm and correlation length $L = 50$ nm. (b) Correction to the measured rms roughness η_m as a function of correlation length of the original two-dimensional exponential surface.

measurement. Specifically, we simulated a two-dimensional rough surface using exponential statistics with varying correlation lengths and rms roughnesses. An example of such a surface with $L = 50$ nm and $\eta = 1$ nm is shown in Fig. 3(a). We then divide the surface into thin segments ($\sim$100 nm) along the y direction and project the two-dimensional surface to obtain a one-dimensional roughness sequence. We repeat this process over 80 segments to obtain an average value of the rms roughness for the projected sequence. This enables us to obtain the correction factor, η_m/η. Figure 3(b) plots the correction factor over the range of correlation lengths measured in our membrane samples. The reduction in rms roughness is severe at short correlation lengths, and the measured rms roughness approaches the actual value only at correlation lengths $\gtrsim$90 nm. Table I contains the corrected rms roughness for our membranes samples. The corrected values are in the range 0.6–1.6 nm.

III. RESULTS AND DISCUSSION

We now discuss the data from the pump-probe measurements. Figure 4 plots the lifetimes for longitudinal acoustic phonon modes excited at different frequencies by varying the thickness of the membrane ($\nu = V_L/2d_0$). The measured phonon lifetimes decrease rapidly from $\tau = 5.4$ ns at $\nu =$ 20.3 GHz to 99 ps at 118 GHz, a nearly two orders of magnitude reduction. We further observe that τ obeys a ν^{-2} dependence in the frequency range $\nu \leqslant 40$ GHz, but this dependence grows stronger, $\tau \sim \nu^{-3}$, at higher frequencies ($\nu \geqslant 60$ GHz).

To understand the frequency dependence of phonon lifetimes, we first consider the intrinsic attenuation of the excited acoustic mode due to interaction with thermal phonons. Depending on the frequency of the acoustic phonon mode and temperature, this interaction can be modeled using the Landau-Rumer [38] or the Akhiezer approach [39]. In the Landau-Rumer model, the interaction of thermal and acoustic phonons occurs via anharmonic three phonon scattering. The theory is valid when $\omega\tau_{\text{th}} \gg 1$, where ω is the angular frequency of the acoustic phonon, and τ_{th} is the thermal phonon relaxation time. In the alternate Akhiezer approach, acoustic phonons act as a driving force to perturb the equilibrium population of thermal phonons. Nonequilibrium phonons collide with each other and remove ordered energy from the acoustic phonon mode as heat. This approach is valid when $\omega \ll k_B T/\hbar$, where k_B is Boltzmann's constant, T is the temperature, and $k_B T/\hbar$ is the average thermal phonon frequency. A fundamental difference between the two approaches is that the Landau-Rumer method evaluates phonon-phonon scattering rates under the single mode relaxation approximation and hence, ignores interactions amongst thermal phonons. The latter significantly affects the attenuation of of an acoustic phonon when $\omega\tau_{\text{th}} \not\gg 1$. For silicon at room temperature, τ_{th} is estimated to be of the

TABLE I. Surface roughness parameters for top and bottom surfaces of membranes.

Thickness (nm)	RMS roughness (nm)	Correlation length (nm)	η_m/η	Corrected RMS roughness (nm)
36	1.2	55	0.85 ± 0.04	1.4
	0.7	6	0.57 ± 0.01	1.2
49	1.3	39	0.81 ± 0.04	1.6
	0.4	8	0.60 ± 0.01	0.7
132	0.8	13	0.66 ± 0.02	1.2
	0.4	9	0.62 ± 0.01	0.6
175	0.6	29	0.77 ± 0.03	0.8
	0.5	14	0.67 ± 0.02	0.7
187	0.6	77	0.87 ± 0.06	0.7
	0.8	24	0.75 ± 0.03	1.0

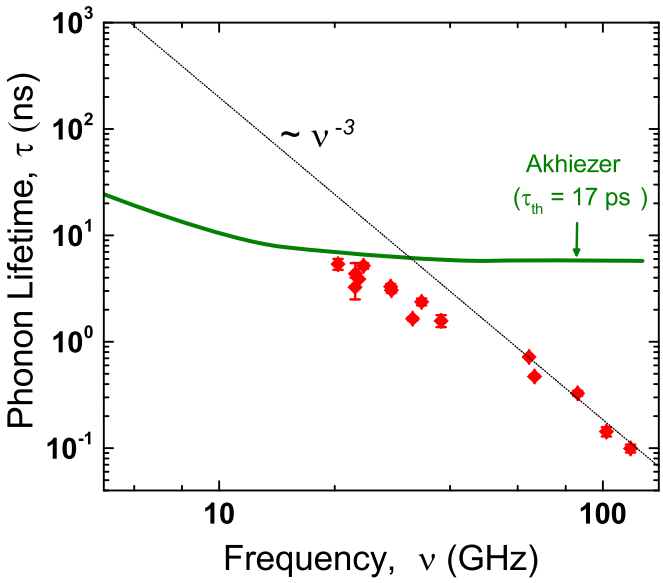

FIG. 4. Lifetimes of longitudinal acoustic phonon modes (♦) excited in thin silicon membranes as a function of frequency. The line labeled Akhiezer is evaluated using Eq. (1) with $\tau_{th} = 17$ ps.

order of tens of picoseconds [19]. The frequency of interest here, ~20–118 GHz, corresponds to the condition $\omega\tau_{th} \sim 1$ and therefore, Akhiezer's model is valid. We use a simplified expression provided by Daly *et al.* [19,40] to evaluate the attenuation of the excited acoustic mode due to Akhiezer

$$\tau_{ph-ph}^{-1} = \frac{CT}{\rho {V_L}^2} \frac{\omega^2 \tau_{th}}{1+\omega^2\tau_{th}^2} (< \gamma^2 > - < \gamma >^2), \quad (1)$$

where C is the volumetric heat capacity, ρ is the density, γ is the grüneisen parameter, and $<>$ denotes an average over all modes. At low frequencies ($\nu \leqslant 24$ GHz), the phonon lifetimes predicted by Akhiezer mechanism (Fig. 4, solid green line) are in close agreement with the measured values. At higher frequencies ($\nu \geqslant 60$ GHz), the Akhiezer model overestimates the data by at least an order of magnitude. The Akhiezer mechanism also predicts nearly a constant value of lifetime over the entire frequency range (20–118 GHz), different from the observed frequency dependence of τ.

Recent work [14] on silicon nanomembranes (<200 nm) suggested that intrinsic scattering based on three phonon interactions instead of Akhiezer damping, are responsible for attenuating frequencies in the range ~20–100 GHz. This is in contradiction of past work on bulk silicon [19] where the Akhiezer model satisfactorily explains lifetimes even at 100 GHz. Since the dispersion relations for thermal phonons in the membranes are identical to those in the bulk, we expect three phonon interactions to be the same as those in the bulk. Indeed, recent atomistic simulations [16] show that modifications to Akhiezer damping occur only in much smaller structures ($\lesssim$10 nm). Finally, with the exception of lowest frequency excited modes ($\nu < 21$ GHz), we measure phonon lifetimes that are nearly an order of magnitude higher than those reported in that work [14], suggesting that the attenuation is not determined by any intrinsic process. We next consider the dominant extrinsic mechanism — boundary scattering.

The excited longitudinal acoustic mode scatters at the surfaces of the film due to surface roughness. Over several reflections, the energy of the coherent excitation diminishes due to out-scattering from the mode. Since we are mainly interested in the coherent part of the excitation that the probe beam senses, we can apply results from wave scattering theory to calculate the damping. In the small perturbation approach [10], the roughness is assumed to introduce a small perturbation to the flat surface profile. In our measurements, this nearly smooth assumption is valid since $\eta/\lambda \lesssim 0.01$. The height of the membrane surface above a reference plane can be described by $\zeta(x,y) = \zeta(\mathbf{r})$, where $<\zeta(\mathbf{r})>= 0$ and $<\zeta^2(\mathbf{r})>= \eta^2$, the rms surface roughness. The perturbation approximation requires that $k_l\zeta \ll 1$ and $\nabla\zeta \ll 1$, where $k_l = 2\pi\nu/V_L$ is the wave vector. From the previous discussion, we assume the autocorrelation function between two points on the surface follows an exponential distribution

$$C(\mathbf{r}) = \frac{1}{\eta^2} < \zeta(\mathbf{R})\zeta(\mathbf{R}+\mathbf{r}) >= e^{-|\mathbf{r}|/L}. \quad (2)$$

The two-dimensional Fourier transform of $C(\mathbf{r})$ is given by

$$\tilde{C}(\mathbf{k}) = \frac{2\pi L^2}{(L^2k^2+1)^{3/2}}. \quad (3)$$

The surface roughness causes a fraction f of the incident longitudinal acoustic phonons to be scattered diffusely into bulk and Rayleigh modes. Following recent work [9] on scattering of elastic waves from boundaries, we consider the spectral surface Green's function $\tilde{G}_{ij}(\mathbf{k},\omega)$ for an elastically isotropic half-space [41,42]. We refer the reader to Maznev's work [9] for a lucid outline and development of the basic wave scattering problem. The scattered fraction, f is given by

$$f = \frac{\eta^2 k_l^3 \rho V_L^2}{\pi^2} \int \tilde{C}(\mathbf{k}) \,\mathrm{Im}\, \tilde{G}_{33}(\mathbf{k},\omega) d\mathbf{k}, \quad (4)$$

where the subscript 3 denotes the direction perpendicular to the surface. It is clear from the above expression that diffuse scattering follows a $\sim\eta^2$ trend but the dependence of f on the correlation length L is not obvious.

For the case of a small correlation length compared to the wavelength of the acoustic mode, $k_l L \ll 1$, Eq. (4) reduces to

$$f_0 \approx \frac{2.84}{\pi s^3}\eta^2 k_l^4 \tilde{C}(\mathbf{k}=0) = \frac{5.68}{s^3}\eta^2 k_l^4 L^2, \quad (5)$$

where $s = V_T/V_L$ is the ratio of transverse and longitudinal acoustic velocity and the subscript "0" denotes small correlation length. In the opposite limiting case of a large correlation length, $k_l L \gg 1$, we obtain

$$f_\infty \approx \frac{1}{\pi^2}\eta^2 k_l^2 \int \tilde{C}(\mathbf{k})\, d\mathbf{k} \; = 4\eta^2 k_l^2. \quad (6)$$

The diffuse scattering fraction shows $\sim L^2$ dependence for $k_l L \ll 1$ but the dependence levels off for $k_l L \gg 1$. To understand the transition between the two limiting cases, we evaluate the integral in Eq. (4) numerically and plot the results in Fig. 5(a). The y axis is normalized by the limiting case of an infinitely long correlation length. Figure 5(a) shows that for $k_l L \gtrsim 5$, the scattering fraction is not sensitive to the actual value of L. At $k_l L \sim 1$, $f \sim 80\%$ of f_∞ and, for $k_l L \geqslant 2$, f is $\geqslant$90% of f_∞. In our data, the deviation from Akhiezer

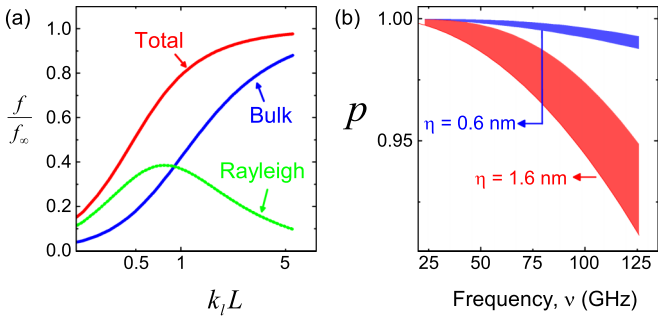

FIG. 5. (a) The diffuse scattering fraction normalized by its value at infinite correlation length, as a function of the product of wave vector and correlation length. The total scattering can be decomposed into individual contributions from bulk and Rayleigh modes. (b) Specularity parameter versus frequency for $\eta = 0.6$ and 1.6 nm and a range of correlation lengths. The upper and lower limit in each shaded region corresponds to $L = 6$ and 77 nm, respectively.

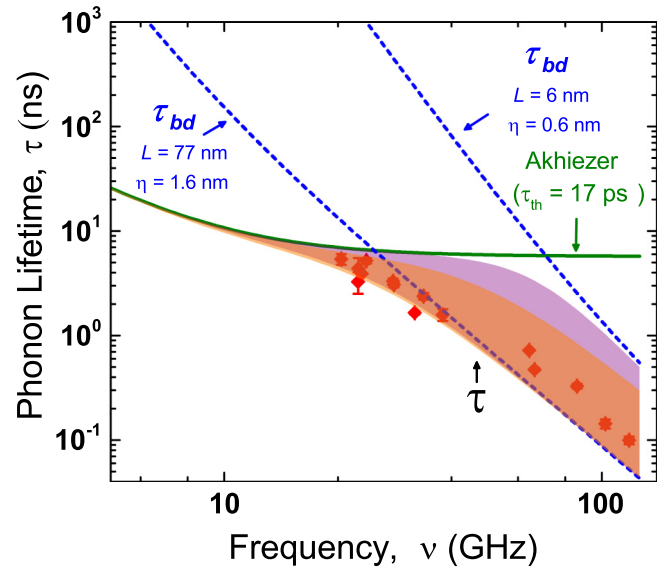

FIG. 6. Boundary scattering and total phonon lifetime calculated using the perturbation approach. The lines labeled τ_{bd} are evaluated using Eq. (7) with $\eta = 0.6$ nm, $L = 6$ nm and $\eta = 1.6$ nm, $L = 77$ nm, respectively. The shaded pink region shows the total phonon lifetime calculated by adding the contribution from Akhiezer and boundary scattering. The shaded orange region shows the phonon lifetime obtained by evaluating the boundary scattering contribution using Ziman's formulation for $\eta \sim 0.6$–1.6 nm.

damping is significant beyond ~60 GHz, where the range of k_l is 0.044–0.088 nm^{-1}. The corresponding range of the product $k_l L$ is ~0.27–6.8 considering that the measured values of correlation length ranges from ~6–77 nm. Figure 5(b) further plots the specularity parameter, $p = 1 - f$, as a function of frequency. We show two shaded graphs for $\eta = 0.6$ nm and $\eta = 1.6$ nm, respectively, corresponding to the smallest and largest rms roughnesses from the measurements. For each rms roughness height, the corresponding shaded regions show the effect of varying the correlation length from 6 to 77 nm. It is evident that we should expect the measured membranes to be closely specular.

We obtain a boundary scattering lifetime τ_{bd} from the specularity parameter as follows. Even though the roughness of the top and bottom sides of the membranes are different, their theoretical specularities are similar (close to 1). Assuming the same value of p for both surfaces, the reduction in energy of the acoustic mode after one round trip over a time, $\Delta t = 2d_0/V_L$ is given by p^2. We therefore obtain

$$\tau_{bd} = \frac{-2d_0}{V_L \ln(p^2)} \approx \frac{d_0}{V_L(1-p)}, \tag{7}$$

where we approximate $\ln(p^2) \approx -2(1-p)$ since p is close to 1, in our structures. We note that the lifetime in Eq. (5) corresponds to the decay of the coherent wave, which is the signal measured by the probe in our experiments. We do not use the expression $\tau_{bd} = (1+p)/(1-p) \times d_0/V_L$ used in previous work [14] that is derived for incoherent transport [43]. The two expressions yield the same value for the range of frequencies reported here but will diverge at higher frequencies when p does not approach 1.

We infer from Eq. (5) that for small correlation lengths ($k_l L \ll 1$), $1 - p \propto \nu^4$. In this limit, the boundary scattering lifetime $\tau_{bd} \approx d_0/V_L(1-p)$ scales with frequency as ν^{-5} due to the inherent frequency-thickness relationship of the membranes, $\nu = V_L/2d_0$. Similarly, for large correlation lengths ($k_l L \gg 1$), the boundary scattering lifetime scales as ν^{-3}. For intermediate $k_l L$, the boundary scattering lifetime obeys $\tau_{bd} \sim \nu^a$ dependence, where $-5 < a < -3$.

Figure 6 replots the phonon lifetime data. The estimated Akhiezer damping time, τ_{ph-ph} is also shown for reference. We use the above theory to plot the boundary scattering lifetime τ_{bd} (dashed blue line) for the range of (L, η) obtained from the HRTEM measurements as $\eta \sim 0.6$–1.6 nm and $L \sim 6$–77 nm. The phonon lifetime τ (shaded pink area) can be estimated using Matthiessen's rule as $\tau^{-1} = \tau_{ph-ph}^{-1} + \tau_{bd}^{-1}$. We find that the data lie within the shaded region across all frequencies. We note that the spread of the shaded area reflects the spread in the statistical parameters of surface roughness. The data agree in magnitude as well as frequency dependence suggesting that phonon boundary scattering is indeed the dominant limiter of lifetimes in our measurements. The data appear more clustered toward the left edge of the shaded region. This may imply that the correlation lengths are longer than what we could measure using the finite window of a TEM. In the limit of infinite correlation length, the specularity given by Ziman's formulation [13] is $p = e^{-16\pi^2\eta^2/\lambda^2}$, independent of the correlation length. Using this expression, we obtain the shaded orange region where the spread is over the range of measured η. We note that the specularity estimated using Ziman's approach and Eq. (6) are essentially identical under the small perturbation approximation ($\eta/\lambda \ll 1$). Further, for the measured range of wave numbers, any correlation length $\gtrsim$130 nm can essentially be considered infinite and would yield a lifetime in the shaded orange region.

As mentioned before, prior measurements on membranes using pump-probe techniques [14] attributed the deviation from Akhiezer damping to three phonon interactions. However, our measurements suggest that the deviation is due to boundary scattering. Further, in measurements using superconducting

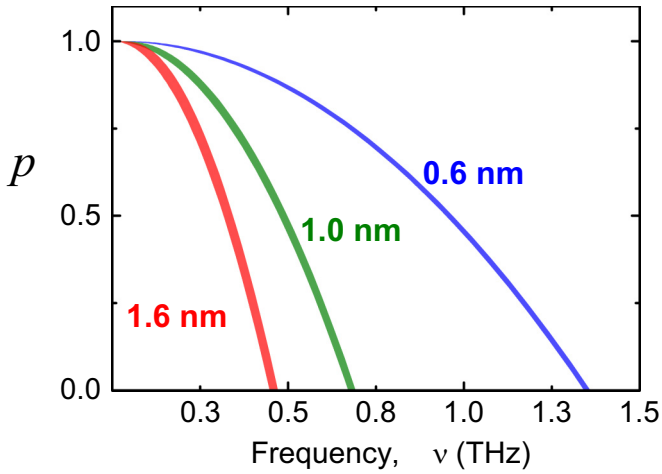

FIG. 7. Specularity parameter versus frequency for $\eta = 0.6$, 1.0, and 1.6 nm. For each shaded region, the upper limit corresponds to $L = 5$ nm, whereas the lower limit corresponds to infinite L.

tunneling junctions (STJs) [11], data could only be explained at zero specularity that was inconsistent with Ziman's expression corresponding to the measured roughness height. In contrast, the data from our work is in excellent agreement with Ziman's expression. As the authors have themselves suggested, the possibility of scattering due to surface contamination or excessive oxidation in the STJ experiments may be responsible for the zero specularity. In either case, our measurements highlight the importance of obtaining detailed surface roughness statistics in order to interpret surface scattering data.

In conclusion, our measurements clearly show that for 60–118 GHz, wave scattering theory agrees well with the data provided detailed roughness statistics are obtained from the measured samples. Consistent with theory, ∼0.1 THz phonons reflect nearly specularly at room temperature from surfaces with ∼1-nm scale roughness. The agreement between theory and data represents an important validation for these theoretical results for phonons. Obtaining detailed surface roughness statistics is key to testing surface scattering theories. In particular, subtle errors in estimating roughness parameters such as the one arising from projecting two-dimensional roughness to one in an HRTEM image can introduce significant errors in theoretical predictions. The frequency range considered here is relevant to damping in nanomechanical resonators and low to intermediate temperature thermal transport. Room temperature thermal transport is dominated by phonons at $\gtrsim$1 THz frequencies which is a more challenging target for future experiments. Figure 7 uses the theory discussed above to calculate the specularity of longitudinal phonons at frequencies higher than those measured here. We note that the assumption of small perturbation is suspect when $\frac{\eta}{\lambda}$ exceeds ∼0.05, which is the case when $p \to 0$ in these calculations. However, the calculations can be considered as an upper bound on specularity. The prediction of a nonzero specularity for a ∼1 THz phonon incident on low-roughness surface presents an interesting target for future investigations. If confirmed experimentally, this might imply that treating surfaces as diffuse scatterers of thermal phonons at room temperature is an overly simplistic assumption.

ACKNOWLEDGMENTS

The authors acknowledge support from the National Science Foundation through Grant No. NSF-CBET-12-50192 and Grant No. NSF-CBET-17-06854.

D.G. and M.G.G. contributed equally to this work.

[1] Y. Ju and K. Goodson, Appl. Phys. Lett. **74**, 3005 (1999).
[2] A. M. Marconnet, M. Asheghi, and K. E. Goodson, J. Heat Transfer **135**, 061601 (2013).
[3] R. Chen, A. I. Hochbaum, P. Murphy, J. Moore, P. Yang, and A. Majumdar, Phys. Rev. Lett. **101**, 105501 (2008).
[4] M. Ghossoub, K. Valavala, M. Seong, B. Azeredo, K. Hsu, J. Sadhu, P. Singh, and S. Sinha, Nano Lett. **13**, 1564 (2013).
[5] J. Lim, K. Hippalgaonkar, S. C. Andrews, A. Majumdar, and P. Yang, Nano Lett. **12**, 2475 (2012).
[6] J. Ma, B. R. Parajuli, M. G. Ghossoub, A. Mihi, J. Sadhu, P. V. Braun, and S. Sinha, Nano Lett. **13**, 618 (2013).
[7] J. Sadhu and S. Sinha, Phys. Rev. B **84**, 115450 (2011).
[8] J. Carrete, L. J. Gallego, L. M. Varela, and N. Mingo, Phys. Rev. B **84**, 075403 (2011).
[9] A. A. Maznev, Phys. Rev. B **91**, 134306 (2015).
[10] J. Ogilvy, Rep. Prog. Phys. **50**, 1553 (1987).
[11] J. B. Hertzberg, M. Aksit, O. O. Otelaja, D. A. Stewart, and R. D. Robinson, Nano Lett. **14**, 403 (2014).
[12] S. O. Rice, Commun. Pure Appl. Math. **4**, 351 (1951).
[13] J. M. Ziman, *Electrons and Phonons: The Theory of Transport Phenomena in Solids* (Oxford University Press, New York, 1960).
[14] J. Cuffe, O. Ristow, E. Chávez, A. Shchepetov, P.-O. Chapuis, F. Alzina, M. Hettich, M. Prunnila, J. Ahopelto, T. Dekorsy, and C. M. S. Torres, Phys. Rev. Lett. **110**, 095503 (2013).
[15] Q. P. Unterreithmeier, T. Faust, and J. P. Kotthaus, Phys. Rev. Lett. **105**, 027205 (2010).
[16] K. Kunal and N. R. Aluru, Phys. Rev. B **84**, 245450 (2011).
[17] P. Mohanty, D. A. Harrington, K. L. Ekinci, Y. T. Yang, M. J. Murphy, and M. L. Roukes, Phys. Rev. B **66**, 085416 (2002).
[18] D. Gelda, J. Sadhu, M. G. Ghossoub, E. Ertekin, and S. Sinha, J. Appl. Phys. **119**, 164301 (2016).
[19] B. C. Daly, K. Kang, Y. Wang, and D. G. Cahill, Phys. Rev. B **80**, 174112 (2009).
[20] A. G. Voronovich, *Wave Scattering From Rough Surfaces*, Vol. 17 (Springer Science & Business Media, New York, 2013).
[21] G. R. Jafari, P. Kaghazchi, R. S. Dariani, A. I. Zad, S. M. Mahdavi, M. R. R. Tabar, and N. Taghavinia, J. Stat. Mech.: Theor. Exp. (2005) P04013.
[22] G. Jafari, S. Mahdavi, A. I. Zad, and P. Kaghazchi, Surf. Interface Anal. **37**, 641 (2005).
[23] A. Shchepetov, M. Prunnila, F. Alzina, L. Schneider, J. Cuffe, H. Jiang, E. I. Kauppinen, C. S. Torres, and J. Ahopelto, Appl. Phys. Lett. **102**, 192108 (2013).

[24] R. M. Costescu, M. A. Wall, and D. G. Cahill, Phys. Rev. B **67**, 054302 (2003).
[25] D. G. Cahill and F. Watanabe, Phys. Rev. B **70**, 235322 (2004).
[26] D. G. Cahill, Rev. Sci. Instrum. **75**, 5119 (2004).
[27] J. R. Goldman and J. A. Prybyla, Phys. Rev. Lett. **72**, 1364 (1994).
[28] O. Wright and V. Gusev, Appl. Phys. Lett. **66**, 1190 (1995).
[29] O. Madelung, M. Schultz, and H. Weiss, Landolt-Bornstein New Series, Group III **17** (1982).
[30] J. Groenen, F. Poinsotte, A. Zwick, C. M. S. Torres, M. Prunnila, and J. Ahopelto, Phys. Rev. B **77**, 045420 (2008).
[31] F. Hudert, A. Bruchhausen, D. Issenmann, O. Schecker, R. Waitz, A. Erbe, E. Scheer, T. Dekorsy, A. Mlayah, and J.-R. Huntzinger, Phys. Rev. B **79**, 201307 (2009).
[32] A. Bruchhausen, R. Gebs, F. Hudert, D. Issenmann, G. Klatt, A. Bartels, O. Schecker, R. Waitz, A. Erbe, E. Scheer, J.-R. Huntzinger, A. Mlayah, and T. Dekorsy, Phys. Rev. Lett. **106**, 077401 (2011).
[33] W. van Dorp, Appl. Phys. A **117**, 1615 (2014).
[34] M. D. Abràmoff, P. J. Magalhães, and S. J. Ram, Biophotonics International **11**, 36 (2004).
[35] G. H. Kruithof, T. M. Klapwijk, and S. Bakker, Phys. Rev. B **43**, 6642 (1991).
[36] S. M. Goodnick, D. K. Ferry, C. W. Wilmsen, Z. Liliental, D. Fathy, and O. L. Krivanek, Phys. Rev. B **32**, 8171 (1985).
[37] T. Yoshinobu, A. Iwamoto, and H. Iwasaki, Jpn. J. Appl. Phys. **33**, 383 (1994).
[38] A. Maradudin and D. Mills, Phys. Rev. **173**, 881 (1968).
[39] A. Akhieser, J. Phys. (USSR) **1**, 277 (1939).
[40] H. J. Maris, Phys. Acoustics **8**, 279 (2012).
[41] A. Maradudin and D. Mills, Ann. Phys. (NY) **100**, 262 (1976).
[42] A. G. Eguiluz and A. A. Maradudin, Phys. Rev. B **28**, 711 (1983).
[43] E. Sondheimer, in *Proceedings of the Royal Society of London A: Mathematical, Physical and Engineering Sciences*, Vol. 203, (The Royal Society, London, 1950), pp. 75–98.

Correction: The previously published Figure 7 had incorrect and missing labels and has been replaced.